applied sciences

MDPI

Article

Probabilistic 4D Trajectory Prediction for UAVs Based on Brownian Bridge Motion

Pengda Zhu [1,2,*], Minghua Hu [1,2], Zexi Dong [1,2] and Jianan Yin [1,2]

[1] College of Civil Aviation, Nanjing University of Aeronautics and Astronautics, Nanjing 211106, China; minghuahu@nuaa.edu.cn (M.H.); zexidong@nuaa.edu.cn (Z.D.); j.yin@nuaa.edu.cn (J.Y.)
[2] State Key Laboratory of Air Traffic Management System, Nanjing University of Aeronautics and Astronautics, Nanjing 211106, China
* Correspondence: zhupengda@nuaa.edu.cn

Abstract

Unmanned aerial vehicle (UAV) flight trajectories in complex environments are often affected by multiple uncertainties, making accurate prediction challenging. To address this issue, this study proposes a probabilistic four-dimensional (4D) trajectory prediction model based on Brownian bridge motion. The UAV's flight from mission start to endpoint is modeled as a Brownian bridge stochastic process with endpoint constraints, where the mean function sequence is constructed from path planning results and UAV performance parameters. To incorporate operational feasibility, the concept of the spatiotemporal reachable domain from time geography is introduced to dynamically constrain reachable positions, while a truncated Brownian bridge distribution is used to model probabilistic positions in three-dimensional space. A simulation platform in a realistic 3D geographical environment is developed to validate the model. Case studies show that the proposed method achieves dynamic probabilistic trajectory prediction under mission constraints with strong adaptability and practicality. The results provide theoretical support and technical reference for trajectory planning, conflict detection, and flight risk assessment in the pre-tactical phase.

Keywords: UAV; trajectory prediction; Brownian bridge motion; spatiotemporal reachability; probabilistic modeling; 4D trajectory

check for updates

Academic Editor: Yutaka Ishibashi

Received: 30 September 2025
Revised: 14 October 2025
Accepted: 15 October 2025
Published: 16 October 2025

Citation: Zhu, P.; Hu, M.; Dong, Z.; Yin, J. Probabilistic 4D Trajectory Prediction for UAVs Based on Brownian Bridge Motion. *Appl. Sci.* **2025**, *15*, 11105. https://doi.org/10.3390/app152011105

Copyright: © 2025 by the authors. Licensee MDPI, Basel, Switzerland. This article is an open access article distributed under the terms and conditions of the Creative Commons Attribution (CC BY) license (https://creativecommons.org/licenses/by/4.0/).

1. Introduction

With the advancement of current technologies and the growing demands for practical applications, unmanned aerial vehicle (UAV) technology has developed rapidly on a global scale, demonstrating significant potential across various domains. Due to their flexibility, low cost, and high efficiency, UAVs are being widely deployed in logistics delivery, security, emergency rescue, environmental monitoring, and other fields. As UAVs become increasingly utilized, trajectory prediction has emerged as a crucial measure to ensure the safety of UAV operations. The results of trajectory prediction are primarily applied in conflict detection [1], mission planning [2], and related areas.

Currently, popular UAV trajectory prediction approaches can be categorized into three types: kinematics-based prediction, state estimation-based prediction, and deep learning-based prediction [3]. Numerous researchers have focused on kinematics-based trajectory prediction. Kalantar et al. [4] modeled UAV trajectories as graphs, where nodes represent positions and edges correspond to possible UAV motion transitions. Path optimization was carried out by considering spatial relationships and connectivity within complex

environments. Guerrero [5] and Ho [6] proposed the use of Kalman filters to combine sensor measurements with predictions from traditional mathematical models, allowing for accurate estimation of the UAV's current state and improvement in prediction precision through periodic updates. Wang [7] and Kant [8] suggested modeling UAV–air interactions using aerodynamic principles to predict UAV trajectories. However, kinematic models tend to be highly sensitive to initial conditions—small errors in these conditions can lead to significant deviations over time, especially in chaotic or nonlinear systems [9]. Moreover, UAVs often operate in complex and dynamic environments, such as urban areas, where interactions with obstacles, other vehicles, and humans are intricate and difficult to model solely with mathematical precision [10]. Additionally, constructing accurate trajectory prediction models using this method requires high-quality training data [11], which may be scarce or difficult to obtain, thereby limiting the model's accuracy and generalizability.

Many researchers have explored trajectory prediction through state estimation methods. Zhao Yifei et al. [12] proposed a Gaussian Process–Unscented Kalman Filter (GP-UKF) hybrid estimation approach based on operational state recognition to improve the accuracy and adaptability of UAV trajectory prediction. Zhang et al. [13] developed a four-dimensional trajectory prediction model using a genetic algorithm, incorporating latitude, longitude, altitude, and entry time into restricted zones. This model extracted parameters such as entry time and number of penetration points to accurately assess potential hazardous intent, thereby enhancing operational safety. Hwang et al. modeled aircraft operational states as hybrid systems, treating trajectory prediction as a state estimation problem of stochastic linear hybrid systems. They introduced the Interacting Multiple Model (IMM) algorithm and the Residual Mean Interacting Multiple Model (RMIMM) algorithm, which incorporates a new likelihood function [14]. Since mode transition probabilities can be modeled as a state-dependent Markov process, Seah, Zhang Junfeng, and others proposed the State-Dependent Transition Hybrid Estimation (SDTHE) algorithm to infer aircraft intent [15], detect potential conflicts [16], and improve mode estimation and trajectory prediction accuracy [17–19].

With the rapid development of machine learning and deep learning, many studies have leveraged large-scale historical data for trajectory prediction. Zhong [20] proposed a short-term four-dimensional (4D) trajectory prediction method based on spatiotemporal trajectory clustering. This method first applied a clustering algorithm to UAV trajectory segments within fixed time windows, assigning each segment a category label representing behavior features such as climbing, turning, or descending. A convolutional neural network (CNN) was then used to identify the behavior category of given segments by learning the associated features. Based on long short-term memory (LSTM) networks, short-term prediction models were developed for each category. Ma et al. [21] proposed a novel method combining CNN and RNN to extract both spatial and temporal features from aircraft trajectories, addressing limitations in earlier RNN-based models. Munaye et al. [22] adopted deep learning techniques, including multilayer perceptrons (MLPs) and LSTM networks, to predict UAV positions and maximize user throughput. Zhang et al. [23] introduced a recurrent-LSTM (RLSTM) algorithm using Automatic Dependent Surveillance-Broadcast (ADS-B) data for accurate trajectory prediction. Simulation results showed that the RLSTM-based method effectively predicted UAV flight trajectories with satisfactory accuracy, addressing the challenge of mid-air conflict avoidance in air traffic control. Zhang Bangchu et al. [24] proposed a trajectory prediction method based on deep LSTM networks. Their results demonstrated that the LSTM model provided low absolute error and high timeliness in trajectory prediction, offering strong technical support for UAV operations in complex air combat scenarios.

In recent years, with increasing airspace complexity and the growing uncertainty of flight missions, probabilistic trajectory prediction has become a prominent research topic. Barratt et al. [25] developed a generative model for aircraft trajectories in airport terminal airspace using radar observation data. They applied time alignment and k-means clustering to construct an efficient Gaussian mixture model, enabling accurate modeling and fast sampling of real trajectory statistical features. Ayhan and Samet [26], from a predictive analytics perspective, divided the airspace into 3D data cubes containing meteorological parameters and employed Hidden Markov Models (HMMs) to model historical trajectories and weather data, thus enabling 4D trajectory prediction under weather uncertainty. Liu and Hwang [16] proposed a 4D trajectory prediction and conflict detection method based on stochastic linear hybrid systems (SLHS), incorporating flight intent information. By modeling the uncertainty of flight mode transitions, they dynamically estimated the probability distribution of future trajectories. Hao Siqi [27] further introduced the concept of time geography, establishing a probabilistic trajectory prediction model that considers pilot intent, 4D flight plan constraints, and spatial obstacle impacts, significantly improving the realism and safety of trajectory predictions. Hu [28] proposes the Probabilistic Multimodal Trajectory Prediction Network (PMTPN), a multitask learning framework that integrates trajectory and probability prediction using multimodal inputs and attention-based motion queries, achieving state-of-the-art accuracy and probabilistic forecasting for vulnerable road users on the JAAD and PIE datasets. Pepper [29] proposes a probabilistic 4D trajectory generation method that integrates lateral path modeling with data-driven climb and descent profiles, enabling realistic and sector-specific aircraft trajectories under uncertainty and outperforming traditional deterministic approaches in airspace simulation. Xiang [30] presents a data-driven trajectory prediction framework combining mixture models and seq2seq neural networks to enhance long-term prediction accuracy and temporal resolution, outperforming existing methods on terminal airspace datasets. Recently, transformer-based and diffusion-based models have achieved notable advances in probabilistic trajectory learning. A recent diffusion-based generative model [31] has shown strong performance in multi-agent trajectory prediction by capturing complex interactions between traffic participants and the environment, while enforcing differential motion constraints to generate diverse and realistic future trajectories. Postnikov [32] proposes a transformer-based baseline model for uncertainty-aware motion prediction of surrounding agents, which effectively captures temporal dependencies and motion uncertainty. Despite its simple and easily implementable architecture, the model demonstrates strong generalization to domain shifts and achieved first-place performance in the 2021 Shifts Vehicle Motion Prediction Competition.

In parallel with these algorithmic advances, the Federal Aviation Administration (FAA) has been refining the Unmanned Aircraft System Traffic Management (UTM) framework to ensure the safe, scalable, and interoperable integration of low-altitude drone operations. According to the FAA [33], UTM represents a collaborative ecosystem built upon regulatory requirements, technical capabilities, and interoperable digital services to manage and mitigate risks associated with unmanned aircraft operations, particularly beyond visual line of sight (BVLOS). The ongoing UTM Operational Evaluation (OE), supported by NASA and industry partners, establishes a federated network of UAS Service Suppliers (USS) and Supplemental Data Service Providers (SDSP) for strategic deconfliction, flight authorization, and risk-informed decision-making. Through the Near-Term Approval Process (NTAP), the FAA evaluates third-party UTM services for safety and interoperability, marking an essential step toward nationwide deployment of cooperative, data-driven airspace management. These developments not only advance the operational maturity of UTM but also emphasize probabilistic trajectory management, automated conflict detection,

and digital coordination between multiple UAV operators—objectives that closely align with the framework proposed in this study.

However, current research still has the following limitations:

(1) In trajectory prediction, the uncertainties faced by UAVs during mission execution are rarely considered. When the flight environment is highly uncertain, it is difficult to obtain a deterministic trajectory.
(2) Most existing prediction methods rely on the availability of large amounts of historical trajectory data, making them unsuitable when such data is lacking.
(3) These studies primarily focus on statistical or correlation-based feature extraction and often lack explicit physical interpretability, making it difficult to ensure kinematic feasibility or compliance with flight performance constraints.

To address these issues, this paper proposes a probabilistic trajectory prediction model for UAVs performing logistics delivery missions in emergency environments, based on Brownian bridge motion. In this model, the UAV's flight process from the mission start point to the endpoint is modeled as a Brownian bridge motion, with the initial planned trajectory treated as the mean function of the Brownian bridge. Meanwhile, by introducing the concept of the spatiotemporal reachable domain from time geography, the model constrains the UAV's possible positions at any given moment, thereby achieving probabilistic trajectory prediction. Furthermore, a realistic three-dimensional geographical environment was constructed in Python 3.11.5, and flight mission simulations were conducted to verify the effectiveness of the proposed probabilistic trajectory prediction model.

2. Probabilistic UAV Trajectory Prediction Model Based on Brownian Bridge Motion

To enable accurate modeling and high-reliability prediction of UAV flight missions in complex environments, this study proposes a probabilistic trajectory prediction model based on Brownian Bridge motion, taking into account the autonomous flight characteristics of UAVs during operations. The UAV's flight from the origin to the destination is modeled as a Brownian Bridge—a stochastic process defined by fixed start and end points. Within this framework, the trajectory is constrained to begin and end at specified locations, exhibiting a bounded random walk over the duration of the flight. This provides an effective means of capturing UAV behavior, where deviations may occur mid-flight, yet the overall path remains constrained by the mission objective.

Furthermore, the planned trajectory—generated according to task requirements and environmental constraints—is treated as the expected path of the Brownian Bridge process. This reflects the reality that UAVs do not fly in a purely random manner; instead, while adhering to a predefined mission route, their actual trajectories may be perturbed by unforeseen factors such as terrain variation, weather disturbances, or the need to avoid other aircraft. Such a modeling approach better reflects the inherent uncertainties of UAV operations, particularly in emergency or dynamic environments.

In addition, this study integrates the concept of the spatiotemporal reachable domain from time geography to constrain the UAV's possible positions at any given time during flight, further enhancing the realism and applicability of the proposed probabilistic prediction model.

2.1. Flight Environment Modeling

Before conducting UAV trajectory planning and four-dimensional trajectory prediction, it is essential to first model the three-dimensional environment in which the UAV mission is executed. This modeling step helps in understanding the operational environment and meeting the obstacle avoidance requirements during flight.

In this study, the UAV mission environment is assumed to be located in mountainous terrain with continuous elevation changes. The modeling of the terrain is achieved using multivariate Gaussian functions. Specifically, two-dimensional Gaussian distributions are used to simulate the height variations of multiple mountain peaks, which are then superimposed to form a complete and realistic terrain model.

The mathematical representation of a natural mountainous terrain can be described as:

$$Z(x,y) = \sum_{i=1}^{N} h_i \, exp\left(-\left(\frac{x - x_{0,i}}{x_{s,i}^2}\right)^2 - \left(\frac{y - y_{0,i}}{y_{s,i}^2}\right)^2\right) \quad (1)$$

In the equation, $Z(x,y)$ represents the terrain elevation of a mountain at location (x,y), N denotes the number of mountain peaks; h_i is the maximum height of the $i-th$ peak,$(x_{0,i}, y_{0,i})$ represents the center coordinates of the $i-th$ peak; and $(x_{s,i}, y_{s,i})$ are the scale parameters of the $i-th$ peak, which determine the spatial extent of the mountain. The term exp denotes the exponential function, which controls the rate of height attenuation. The three-dimensional geographic environment model is illustrated in Figure 1.

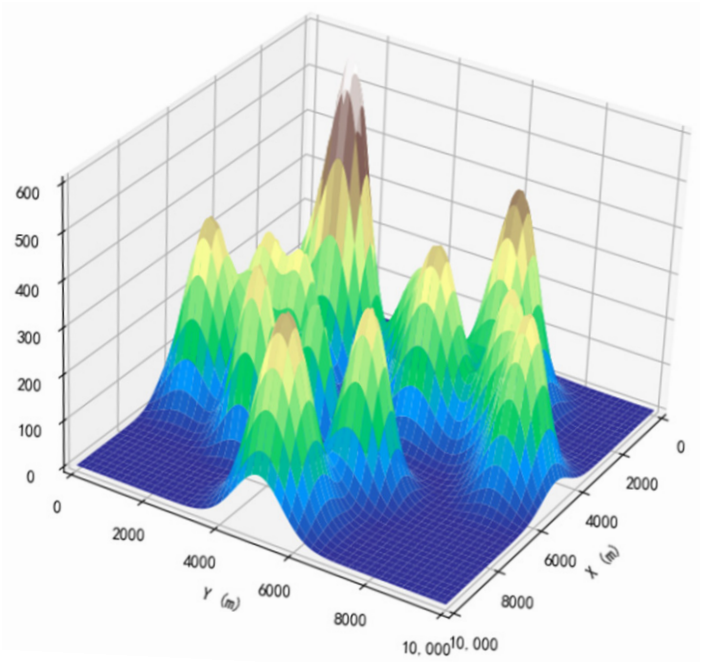


Figure 1. Three-dimensional Geographic Environment.

2.2. Initial Flight Path Planning

Considering the complexity of mountainous environments in which UAV missions are carried out, this study adopts an improved A* algorithm to perform three-dimensional path planning for UAV flight. The A* algorithm [34] is a widely used pathfinding algorithm capable of identifying the shortest path between two points within a graph or 3D space. In the constructed 3D geographic environment, the A* algorithm searches for the optimal path by combining a heuristic function with the actual cost. It incrementally explores potential paths from intermediate nodes to the target point while simultaneously tracking the best path identified so far.

In complex and large-scale three-dimensional environments, the integration of a heuristic function allows the A* algorithm to maintain optimality while significantly improving search efficiency. The cost function of the A* algorithm is expressed as:

$$f(n) = g(n) + h(n) \tag{2}$$

In the cost function, $g(n)$ represents the actual cost from the starting point to the intermediate node n, while $h(n)$ denotes the heuristic estimated cost from node n to the goal. In three-dimensional environments, the heuristic is typically based on either Euclidean distance or Manhattan distance. And the total cost then is given by $f(n)$.

In conventional 3D A* algorithms, using only the Euclidean distance as the heuristic function may lead to an underestimation of the actual path cost, as it overlooks directional movement constraints inherent in grid-based navigation. This can result in reduced search efficiency and inaccurate path estimation.

To address these limitations, the improved A* algorithm in this study, we designed the heuristic function $h(n)$ as a weighted combination of three distance metrics: Euclidean distance, Manhattan distance, and Chebyshev distance. The Euclidean distance is defined as: $h_1(n) = \sqrt{(x_n - x_g)^2 + (y_n - y_g)^2 + (z_n - z_g)^2}$, where x_n, y_n, z_n are the coordinates of the current node n, and x_g, y_g, z_g are the coordinates of the goal node. The Euclidean distance accurately represents the straight-line distance between two points in continuous space and is particularly effective when the object is free to move in any direction. The Manhattan distance is given by the following: $h_2(n) = |x_n - x_g| + |y_n - y_g| + |z_n - z_g|$, Manhattan distance is well-suited for grid environments with axis-aligned movement, helping to constrain the search direction and reduce unnecessary expansions. The Chebyshev distance is expressed as: $h_3(n) = \max(|x_n - x_g|, |y_n - y_g|, |z_n - z_g|)$, This metric is applicable in scenarios where diagonal or multi-directional movement is allowed, and it effectively estimates the minimum number of steps required when movement along multiple directions is permitted simultaneously.

By combining these three distance metrics with appropriate weights, the heuristic function can fully account for various movement constraints and environmental characteristics. This ensures accurate cost estimation while enhancing search efficiency and adaptability. The final expression for the improved heuristic cost is given by the following:

$$h(n) = w_1 h_1(n) + w_2 h_2(n) + w_3 h_3(n) \tag{3}$$

In Equation (3), w_1, w_2, w_3 are the weighting coefficients of the heuristic function, subject to the constraint $w_1 + w_2 + w_3 = 1$. To further improve the efficiency of the improved A* algorithm, a parameter search method was employed to systematically determine the optimal weight combination, as the heuristic weights directly influence both computational efficiency and path optimality.

Starting from the initial weights (0,0,1), the search iteratively adjusted the coefficients with a step size of 0.1, generating 100 candidate configurations in total. For each configuration, experiments were conducted to compare the resulting path length and computation time. The optimal set of heuristic weights was empirically identified as $w_1 = 0.1$, $w_2 = 0.3, w_3 = 0.6$ [35].

This configuration enables the heuristic function to better handle complex environments with varying motion constraints, achieving a balanced trade-off between search accuracy and efficiency. Experimental results confirm that the improved A* algorithm with these optimized weights exhibits superior pathfinding performance in three-dimensional UAV flight environments.

Compared to the traditional A* algorithm, this approach integrates multiple distance measures to construct a more adaptive heuristic function, which not only improves the accuracy of path estimation but also enhances search efficiency and practical usability—especially in complex terrain scenarios involving 3D UAV flight path planning.

In conventional A* implementations, node expansion typically involves iterating through all neighboring nodes of the current position and evaluating their associated costs. While this exhaustive approach ensures completeness, it often leads to redundant expansions in dense or sparse areas, increasing computational overhead. To address this issue and improve search efficiency, this study introduces a jump expansion strategy, which continuously searches in a given direction until a valid node meeting the constraints is encountered. This effectively skips redundant intermediate nodes and enables rapid path advancement. The strategy is inspired by the core principles of the Jump Point Search (JPS) algorithm and significantly reduces the number of expanded nodes, narrows the search space, and improves computational efficiency in 3D path planning within complex environments.

When applying this improved A* algorithm for path planning in a 3D geographic environment, it is first necessary to discretize the environment through voxelization, transforming it into a structured 3D grid. The 3D space is divided into uniformly sized cubic cells (voxels). Any cell that intersects with an obstacle is marked as unavailable, facilitating obstacle identification during the planning process. After voxelization, each grid cell may consider up to 26 neighboring cells—including cells in axial, face-diagonal, and body-diagonal directions—as candidate nodes for expansion during the search process.

To eliminate abrupt changes in the discrete path generated during A* path planning and to enhance the smoothness and flight feasibility of the resulting path—thereby facilitating the generation of an initial four-dimensional trajectory—this study applies a post-processing smoothing technique based on iterative averaging. Assume the initial path consists of N three-dimensional coordinate points, denoted as $P = \{P_0, P_0, \ldots, P_{N-1}\}$, where each point $p_i = (x_i, y_i, z_i)^T$. Under the constraint that the start and end points remain unchanged, all intermediate points are smoothed iteratively using the following update formula: $p_i^{(t+1)} = p_i^{(t)} + \alpha\left(\frac{p_{i-1}^{(t)} + p_{i+1}^{(t)}}{2} - p_i^{(t)}\right)$, $i = 1, 2, \ldots, N-2$, Here, $\alpha \in (0,1)$ is the smoothing factor that controls the strength of smoothing, and in this study, α is set to 0.3. The variable t represents the iteration number, with the number of iterations set to 100 to ensure sufficient smoothness. This formula essentially implements a Laplacian smoothing approach driven by local averaging. Each intermediate point is gradually adjusted toward the average of its neighboring points, reducing high-frequency variations in the path and improving its overall smoothness. After multiple iterations, a geometrically smoother and continuous path suitable for UAV flight is obtained, laying the foundation for subsequent altitude safety adjustments and four-dimensional trajectory prediction.

The improved A* algorithm used in this study follows a general path search framework consisting of four main steps: initialization, node expansion, cost evaluation, and path backtracking. The detailed steps are as follows:

Step 1: Initialization

First, the positions of the start and goal points are determined, with the start point designated as the initial search node. Initialize the path cost function by setting the cumulative cost from the start node to the current node to zero. Then, compute the heuristic estimate from the start node to the goal node, and use the sum of these two values as the total cost. This total cost serves as the evaluation criterion for subsequent node selection.

Step 2: Node Expansion and Jump Search

In the main search loop, the node with the minimum total cost is selected from the candidate set as the current expansion node. If this node corresponds to the goal, the search terminates. Otherwise, the algorithm proceeds to expand nodes from the current position in all 26 neighboring directions within the 3D space. Unlike traditional A*, which incrementally evaluates each neighbor, the proposed method introduces a jump search

strategy, where the search proceeds in each direction until a valid node that satisfies feasibility constraints is encountered. This approach skips over intermediate invalid regions, significantly reducing redundant expansions and improving search efficiency.

Step 3: Cost Evaluation and Node Update

For each feasible node reached via jump expansion, the cumulative cost from the start point is computed, and the heuristic cost is re-evaluated. The heuristic function used here is a weighted combination of Euclidean, Manhattan, and Chebyshev distances, which balances path optimality, directional constraints, and 3D spatial expansion characteristics. If the newly calculated path is better than the previously recorded one, the node's minimum cost and predecessor information are updated, and the node is added to the candidate set for further exploration.

Step 4: Path Backtracking and Extraction

Upon first reaching the goal node, the algorithm reconstructs the complete path by backtracking through the chain of predecessor nodes, ultimately forming the full path sequence from start to goal. The resulting path serves as the initial output of UAV flight trajectory planning and is subsequently refined through smoothing and used for flight safety validation.

2.3. Spatiotemporal Reachable Set

To accurately represent the feasible flight space of unmanned aerial vehicles (UAVs) during four-dimensional (4D) trajectory prediction—under the joint influence of kinematic constraints, time limitations, and terrain restrictions—this study introduces the concept of the Spatiotemporal Reachable Set (STRS), grounded in the theory of time geography. The STRS at a given time $t \in [0, T]$ is defined as the set of all spatial positions that a UAV can reach from its starting point, within its physical performance limits (such as maximum speed and acceleration), and from which it can still arrive at the destination within the remaining time.

Building upon this, 3D terrain data and obstacle avoidance requirements are integrated to construct the constrained boundaries of the feasible flight region. These boundaries are used to confine the probability distribution during the trajectory prediction process.

In practical mission execution scenarios, the UAV's departure time, starting location, destination, and task deadline are typically predefined. Therefore, under the constraints of the mission time window and flight performance, the UAV's reachable spatial domain at any given moment is inherently limited. Geographic regions outside this domain are considered unreachable at that time, thereby forming the STRS for the UAV at the corresponding time point.

Moreover, this study focuses on UAV logistics delivery missions conducted in emergency scenarios. In such contexts, UAVs typically do not follow strictly predefined trajectories; instead, their flight paths are dynamically adjusted in response to factors such as weather conditions and changes in the geographic environment. Therefore, constructing a spatiotemporal reachable set (STRS) based on mission objectives and terrain constraints not only provides a theoretical boundary for dynamic 4D trajectory planning but also offers practical support and physically grounded constraints for subsequent probabilistic trajectory prediction. This approach plays a crucial role in enhancing the accuracy and reliability of trajectory forecasting.

At prediction time t, considering the UAV's maximum horizontal speed V_{max}, the maximum horizontal distance it can reach from the starting point (x_s, y_s) is given by the following:

$$R_{start}(t) = V_{max} \cdot t \tag{4}$$

During the remaining time, the UAV must be able to reach the destination point (x_g, y_g); therefore, the maximum allowable distance between the current position and the destination is as follows:

$$R_{goal}(t) = V_{max} \cdot (T - t) \tag{5}$$

Thus, the two-dimensional spatial reachability constraint at time t can be expressed as:

$$\begin{cases} (x - x_s)^2 + (y - y_s)^2 \leq R_{start}^2(t) \\ (x - x_g)^2 + (y - y_g)^2 \leq R_{goal}^2(t) \end{cases} \tag{6}$$

This constraint defines the feasible region at time t in which the UAV can both be reached from the starting point and continue on to the destination within the remaining time, considering horizontal movement.

In the context of four-dimensional trajectory prediction for UAVs, the spatiotemporal reachable set is influenced not only by the temporal and spatial constraints of the start and end points, but also by obstacle avoidance requirements imposed by the surrounding geographical environment at the current location. To ensure flight safety, terrain-based obstacle avoidance conditions must be incorporated into the definition of the reachable set. Let $u_z(t)$ denote the UAV's expected flight altitude at time t, and let Δh be the predefined safety margin that ensures a minimum safe clearance between the flight trajectory and the terrain. The terrain contour boundary is then defined as:

$$h(x, y) = u_z(t) - \Delta h \tag{7}$$

Here, $h(x, y)$ represents the terrain elevation at any given location on the two-dimensional plane. The corresponding contour line defines the set of positions where the terrain height exactly reaches the minimum allowable flight altitude, given by the current flight altitude minus the safety margin. Therefore, only the regions within this boundary that satisfy the condition $h(x, y) \leq u_z(t) - \Delta h$ are considered to meet the obstacle avoidance requirements and are included in the UAV's safe reachable area at time t.

By combining the terrain-based obstacle avoidance constraints with the previously defined spatiotemporal constraints determined by the start and end points, the final composite spatiotemporal reachable set is obtained. This set defines the UAV's reachable space at each prediction time, subject to time constraints, physical performance limitations, and environmental safety conditions:

$$R_t^{final} = R_t^{physical} \cap R_t^{geography} \tag{8}$$

2.4. Brownian Bridge-Based 4D Trajectory Prediction Model

For UAVs performing flight missions, it is assumed that although the mission must be completed within a specified time window, the UAV does not strictly follow a pre-planned trajectory during the mission. Instead, it exhibits a certain degree of autonomy. When operating in unfamiliar geographic environments for the first time, the UAV may deviate from the planned trajectory due to adverse weather conditions or environmental disturbances encountered during flight. For such missions—characterized by limited prior information—the UAV's motion can be viewed as a form of random walk [30].

Therefore, this study adopts Brownian bridge motion to model UAV flight behavior under emergency conditions.

The Brownian Bridge is a continuous-time stochastic process $B(t)$, which, under the conditions $B(0) = B(1) = 0$, follows the conditional probability distribution of a Wiener process $W(t)$ [28]. Accordingly, when the motion process is strictly constrained at both the start and end points, the Brownian Bridge model can effectively describe the motion characteristics of the system.

Suppose the UAV departs from the starting point (x_s, y_s) at time t_s, and after a planned period of flight, arrives at the destination (x_g, y_g) at time t_g. Then, according to the standard Brownian Bridge model, the UAV's position at any time $t \in (t_s, t_g)$ follows the distribution:

$$\begin{bmatrix} x(t) \\ y(t) \end{bmatrix} \sim N\left(\begin{bmatrix} \mu_x(t) \\ \mu_y(t) \end{bmatrix}, \begin{bmatrix} \sigma_X^2(t) & 0 \\ 0 & \sigma_Y^2(t) \end{bmatrix} \right) \tag{9}$$

$$\mu_x(t) = \frac{(t - t_s)x_g + (t_g - t)x_s}{t_g - t_s} \tag{10}$$

$$\mu_y(t) = \frac{(t - t_s)y_g + (t_g - t)y_s}{t_g - t_s} \tag{11}$$

$$\sigma_x^2(t) = \sigma_y^2(t) = \frac{(t - t_s)(t_g - t)}{t_g - t_s} \tag{12}$$

In the above formulation:

$\mu_x(t)$—the expected value of the UAV's position in the x—direction at time t.

$\mu_y(t)$—the expected value of the UAV's position in the y—direction at time t.

$\sigma_x^2(t)$—the variance of the UAV's deviation from the mean in the x—direction at time t.

$\sigma_y^2(t)$—the variance of the UAV's deviation from the mean in the y—direction at time t.

These expressions indicate that, in a standard Brownian Bridge process, the expected position always lies on the straight line connecting the start and end points, and the distance from the expected position to the start point varies linearly with time. Moreover, the variance is zero at both the starting and ending times, and reaches its maximum value during the middle of the flight interval.

Given that UAV missions typically involve long travel distances, complex terrain, and real-time obstacle avoidance requirements, the assumption in the standard Brownian Bridge model—where the expected trajectory is simplified as a straight line between the start and end points—is inadequate for this study. Therefore, in this paper, the expected trajectory of the Brownian Bridge is defined using the planned flight path, which is generated based on task requirements and 3D environmental constraints. By incorporating UAV performance parameters, a time-stamped 4D trajectory is constructed, which is then used to determine the Brownian Bridge's expected position functions $\mu_x(t)$ and $\mu_y(t)$ at each time step.

The expected trajectory proposed in this study is generated based on the UAV's physical performance characteristics and the results of path planning. The following assumptions are made regarding the UAV's motion model: the UAV adopts a piecewise motion model in both the horizontal and vertical directions, consisting of three fundamental motion states—uniform motion, uniform acceleration, and uniform deceleration. Specifically, the takeoff and landing phases involve acceleration and deceleration, respectively, while the cruise phase maintains a constant velocity.

Based on the pre-planned 3D safety trajectory, horizontal motion parameters are introduced, including the horizontal cruising speed v_h and horizontal acceleration a_h. Using these parameters, the required time for acceleration is computed as $t_{acc} = \frac{v_h}{a_h}$, and the corresponding acceleration distance as $d_{acc} = 0.5 a_h t_{acc}^2$.

After calculating the cumulative travel distance s on the horizontal plane for each trajectory point, the entire flight process is divided into three stages based on the relationship between s and the total horizontal distance s_{total}. Acceleration phase: For points where $s \leq d_{acc}$, the corresponding time is computed using the kinematic equation $t = \sqrt{\frac{2s}{a_h}}$. Constant-speed phase: For points where $d_{acc} < s < S_{total} - d_{acc}$, time is assigned linearly as $t = t_{acc} + \frac{s - d_{acc}}{v_h}$. Deceleration phase: Near the destination, the remaining travel distance is used to derive the deceleration time in reverse, and time values are assigned progressively to each trajectory point.

This piecewise calculation method yields a time sequence that corresponds one-to-one with the 3D spatial positions, thereby forming a discrete four-dimensional trajectory $\mu_x(t)$, $\mu_y(t)$, $\mu_z(t)$, where each trajectory node contains four dimensions: (x, y, z, t). To further enhance the smoothness and continuity of the trajectory in the temporal dimension, this study applies cubic spline interpolation to smooth the discrete time nodes and their corresponding spatial coordinates. The resulting continuous 4D trajectory not only accurately reflects the UAV's spatial movement characteristics but also satisfies basic dynamic constraints in the time domain. This expected 4D trajectory serves as a solid foundation for the subsequent probabilistic trajectory prediction based on Brownian Bridge motion.

Based on the above, the final expression for the UAV's position distribution on the horizontal plane, modeled using Brownian Bridge motion, is given as:

$$p_{orig}(x, y|t) = x(t)y(t) = \frac{1}{2\pi\sigma_{xy}(t)^2} exp\left[-\frac{(x - \mu_x(t))^2 + (y - \mu_y(t))^2}{2\sigma_{xy}(t)^2}\right] \tag{13}$$

In the above formula $\mu_x(t), \mu_y(t)$ denote expected 4D trajectory.

However, the position distribution derived from the Brownian Bridge model is unconstrained—meaning it may include positions that lie outside the UAV's spatiotemporal reachable set or violate obstacle avoidance requirements. To address this issue, the previously defined spatiotemporal reachable set must be applied to constrain the Brownian Bridge-based position distribution. Specifically, the probability of any position falling outside the reachable domain at a given time should be set to zero. Directly discarding the out-of-domain probabilities, however, leads to distortions in the normalized probability distribution at each time step. Therefore, in this study, a truncated distribution is adopted to accurately describe the constrained position distribution under the Brownian Bridge framework.

As described in Section 2.3, let $\Omega(t)$ denote the set of all positions at time t that satisfy the constraints of the final spatiotemporal reachable domain R_t^{final}. That is, for any given point, if it satisfies all constraints of the reachable domain, then $(x, y) \in \Omega(t)$; otherwise, $(x, y) \notin \Omega(t)$.

To facilitate the mathematical formulation, we introduce the indicator function $\tau_{\Omega(t)}$:

$$\tau_{\Omega(t)} = \begin{cases} 1, \ if(x, y) \in \Omega(t) \\ 0, \ if(x, y) \notin \Omega(t) \end{cases} \tag{14}$$

This indicator function is used to filter out points within the feasible domain, effectively truncating the probability values of points outside the domain to zero.

Let Equation (13) denote the original position distribution of the Brownian Bridge model at time t, denoted as $p_{orig}(x, y|t)$. By truncating this distribution outside the spa-

tiotemporal reachable domain $\Omega(t)$ and re-normalizing it within the domain, the truncated distribution is defined as:

$$p_{trunc}(x, y|t) = \frac{p_{orig}(x, y|t)\tau_{\Omega(t)}}{\iint_{\Omega(t)} p_{orig}(u, v|t)dudv} \tag{15}$$

In the above equation the denominator serves as the normalization constant, ensuring that the truncated distribution integrates to 1 over the domain $\Omega(t)$:

$$\iint_{\Omega(t)} p_{trunc}(x, y|t)dxdy = 1 \tag{16}$$

Thus, the final position distribution of the UAV on the horizontal plane, constrained by the Brownian Bridge model and spatiotemporal reachability, is given by the following:

$$p(x, y|t) = p_{trunc}(x, y|t) \tag{17}$$

To further account for the UAV's deviation from the expected trajectory in the vertical (altitude) direction, this study models the vertical position using a truncated normal distribution. Specifically, based on flight safety requirements and UAV performance limitations, the allowable altitude range is defined as:

$$\left[z_{lower}, z_{upper}\right] = [\max(0, \mu_z(t) - \Delta h_1), \mu_z(t) + \Delta h_2] \tag{18}$$

where $\mu_z(t)$ is the expected altitude obtained from the interpolated 4D trajectory, and the lower bound $\max(0, \mu_z(t) - \Delta h_1)$ ensures that the UAV does not fly below ground level or below a minimum safety margin. The upper bound $\mu_z(t) + \Delta h_2$ limits the UAV from flying excessively high.

To construct the truncated normal distribution, the standard deviation is defined based on the width of the allowable interval as:

$$\sigma_z = \frac{z_{upper} - z_{lower}}{4} \tag{19}$$

This formulation reflects the degree of uncertainty in altitude distribution within the permitted range. Applying standard normalization techniques, the lower and upper bounds are expressed in standardized form as:

$$a_z = \frac{z_{lower} - u_z(t)}{\sigma_z}, b_z = \frac{z_{upper} - u_z(t)}{\sigma_z} \tag{20}$$

Using the truncated normal distribution model, the probability density function for altitude at time t within the interval $\left[z_{lower}, z_{upper}\right]$ is given by the following:

$$p(z|t) = \frac{\varnothing\left(\frac{z-u_z(t)}{\sigma_z}\right)}{\sigma_z[\Phi(b_z) - \Phi(a_z)]}, \; z \in \left[z_{lower}, z_{upper}\right] \tag{21}$$

where $\varnothing(\cdot)$ and $\Phi(\cdot)$ denote the probability density function (PDF) and cumulative distribution function (CDF) of the standard normal distribution, respectively. For numerical implementation, the allowed altitude interval is uniformly discretized, and numerical integration techniques are employed to compute the truncated normal PDF. The resulting values are then normalized to ensure that the total probability across the allowable altitude range equals 1 at each time step.

At this point, we have obtained: the horizontal position distribution $p(x, y|t)$ based on the Brownian Bridge model, and the vertical position distribution $p(z|t)$ based on the truncated normal model. Accordingly, the joint probability that the UAV is located at position (x, y, z) at time t, under the constraints of the spatiotemporal reachable domain, is given by the product of the two marginal distributions:

$$prob(x, y, z) = p(x, y|t) \times p(z|t) \tag{22}$$

3. Case Study

To validate the feasibility and effectiveness of the proposed probabilistic UAV trajectory prediction model based on Brownian Bridge motion, a simulation was conducted in a Python environment to model the UAV mission's geographic environment and implement the trajectory prediction algorithm.

3.1. Simulation Environment and Parameter Settings

A mountainous terrain was simulated as the operational environment for the UAV mission. A square area of 10 km × 10 km with a maximum elevation of 700 m was generated. The terrain was constructed by superimposing multiple Gaussian-shaped peaks. In this scenario, the UAV is assumed to be performing an emergency logistics delivery mission, with the starting point located at (1000, 9000) and the destination at (9000, 2000).

According to the probabilistic trajectory prediction framework described above, the Brownian Bridge-based model requires an initial path planning phase to define the UAV's mission trajectory. First, the 3D environment is discretized to form a three-dimensional grid-based search space. The horizontal plane is divided uniformly in both the x and y directions. Specifically, the horizontal region spans [0, 10,000] meters with a resolution of 200 × 200, resulting in a grid spacing of approximately 50 m. The vertical range extends from 0 to 700 m, discretized into 250 layers, giving a vertical grid resolution of about 2.8 m.

Each grid node is denoted as (i, j, k), corresponding to actual spatial coordinates (x_j, y_j, z_k). To ensure flight safety, all navigable grid nodes (except those used for takeoff and landing) must satisfy a minimum altitude clearance condition given by the following: $Z_k \geq Z(i, j) + H_{clearance}$, where $Z(i, j)$ is the terrain height at grid location (i, j), and $H_{clearance}$ is the minimum safety altitude threshold. To avoid misjudgment of grid availability due to abrupt terrain changes, the clearance value is chosen to be greater than the vertical grid height; in this study, $H_{clearance}$ is set to 4 m. Additionally, buffer zones with a radius $r = 3$ grids are introduced around both the starting and ending points. These zones allow takeoff and landing operations to occur even if the safety clearance is not strictly satisfied, thereby enhancing the practical feasibility of the algorithm. Based on the setup above, the initial path planning for the UAV is generated using the improved A* algorithm, and the resulting trajectory is shown in the Figure 2 below.

After obtaining the UAV's initial planned path, the expected four-dimensional (4D) trajectory is derived based on the UAV's physical cruising characteristics. The UAV used in this study is the SF Express Ark 80, designed for logistics delivery missions. This UAV has a cruising speed of 14 m/s, a vertical acceleration of approximately 2–4 m/s^2, a horizontal acceleration range of 2–5 m/s^2, and a maximum flight speed of up to 30 m/s. In the simulation, the UAV's cruising speed is set to 14 m/s, and both vertical and horizontal accelerations are taken as 4 m/s^2. Using these parameters, a time-stamped 4D trajectory is constructed. A visual representation of the expected 4D trajectory, plotted at two-minute intervals, is shown in the Figure 3 below.

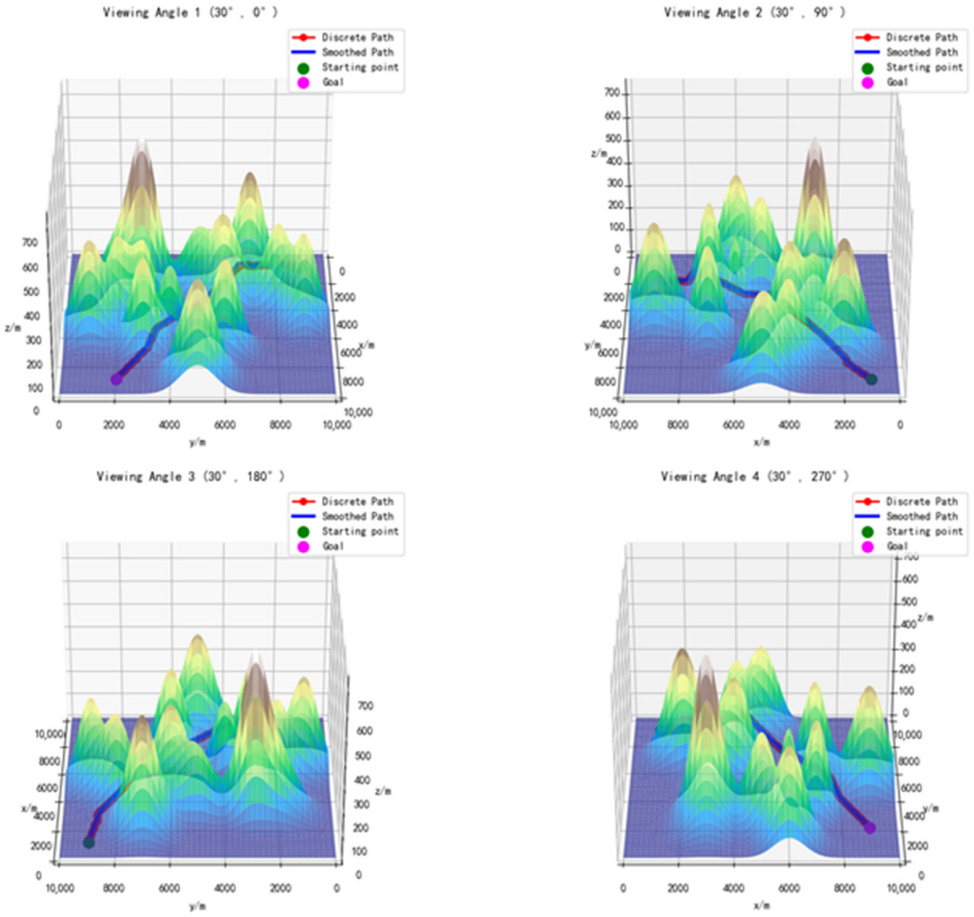


Figure 2. Initial path planning of the drone.

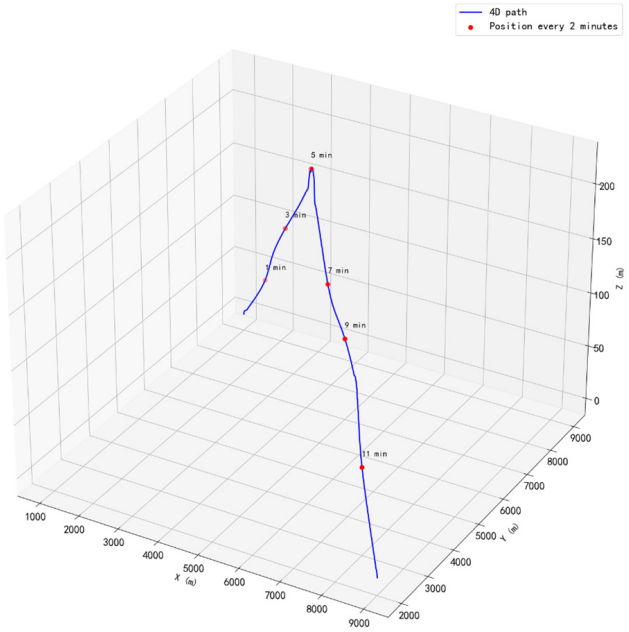


Figure 3. Expected 4D trajectory of the UAV.

3.2. Spatiotemporal Reachable Domain Visualization

Before performing four-dimensional (4D) trajectory prediction, it is necessary to compute the spatiotemporal reachable domain at each time step. In the simulation, the UAV's maximum speed is set to $v_{max} = 17$ m/s. When determining the terrain contour boundary using the condition $h(x, y) = u_z(t) - \Delta h$, the safety margin is set to $\Delta h = 3$ m. That is, the

terrain boundary is defined as the set of locations where the elevation equals 3 m below the UAV's expected altitude at the current position. This constraint further reduces the size of the UAV's spatiotemporal reachable set, ensuring strict compliance with obstacle avoidance requirements. A visual illustration of the spatiotemporal reachable domain during the UAV's flight is shown in the figure below.

Before conducting four-dimensional trajectory prediction, it is necessary to determine the spatiotemporal reachable domain (STR) at each moment. When solving the UAV's STR, directly using the mission's starting point as the origin for the reachable domain at any moment may lead to excessively large results, deviating from the UAV's actual flight path and becoming inconsistent with its real operating conditions, especially when the mission's starting and ending points are far apart.

Therefore, in this study, when calculating the STR, the expected four-dimensional trajectory coordinate 30 s before the given moment is taken as the starting point, ensuring reachability from the origin. Meanwhile, the expected four-dimensional trajectory coordinate 30 s after that moment is used as the endpoint, ensuring that the UAV can reach the destination within the prescribed time. This method provides a more accurate representation of the UAV's actual operation.

In the simulation, the UAV's maximum speed is set as $v_{max} = 17$ m/s, For the terrain contour boundary, we use $h(x, y) = u_z(t) - \Delta h$, where $\Delta h = 3$ m, meaning the terrain contour line corresponding to 3 m below the UAV's expected altitude at the current position. This further narrows the UAV's reachable domain and strictly satisfies the obstacle avoidance requirement.

The schematic diagram of the UAV's spatiotemporal reachable domain during the flight process is shown below in Figure 4:

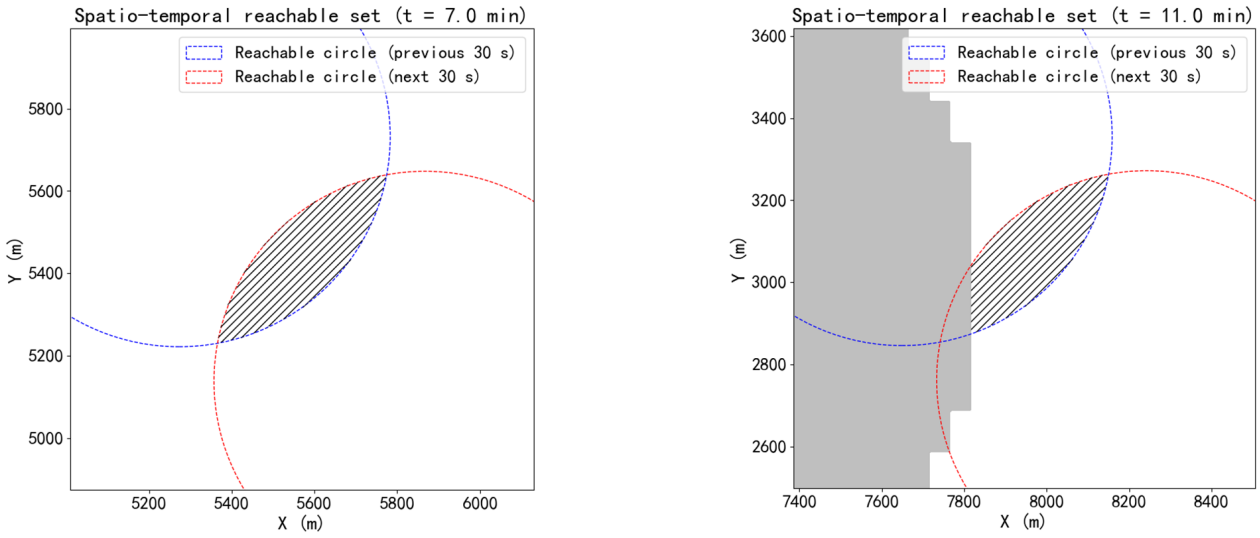


Figure 4. Spatiotemporal Reachable Set of the UAV.

In the schematic diagram of the reachable domain, the blue circle represents the reachable region when the UAV flies from the starting point at its maximum speed, while the red circle represents the spatiotemporal reachable domain that satisfies the requirement of reaching the destination within the prescribed time at maximum speed. The gray shaded area indicates obstacle regions where the UAV's expected four-dimensional trajectory does not meet the required safety altitude at the current moment; to ensure flight safety, the UAV must not enter this area. The hatched shaded region represents the UAV's final spatiotemporal reachable domain at the current moment.

3.3. Probabilistic 4D Trajectory Prediction Results

Finally, probabilistic trajectory prediction of the UAV is carried out based on Brownian bridge motion. According to the above results, the UAV departs from the mission starting point at 00:00:00 with 3D coordinates (1000, 9000, 0) and arrives at the mission destination at 00:12:47 with coordinates (9000, 2000, 0). Based on the four-dimensional trajectory prediction model constructed with Brownian bridge motion during the modeling process, the UAV's positional probability distribution on the XY plane is first calculated according to Equation (17). The probability distribution of the drone's position on the XY plane is shown in Figure 5.

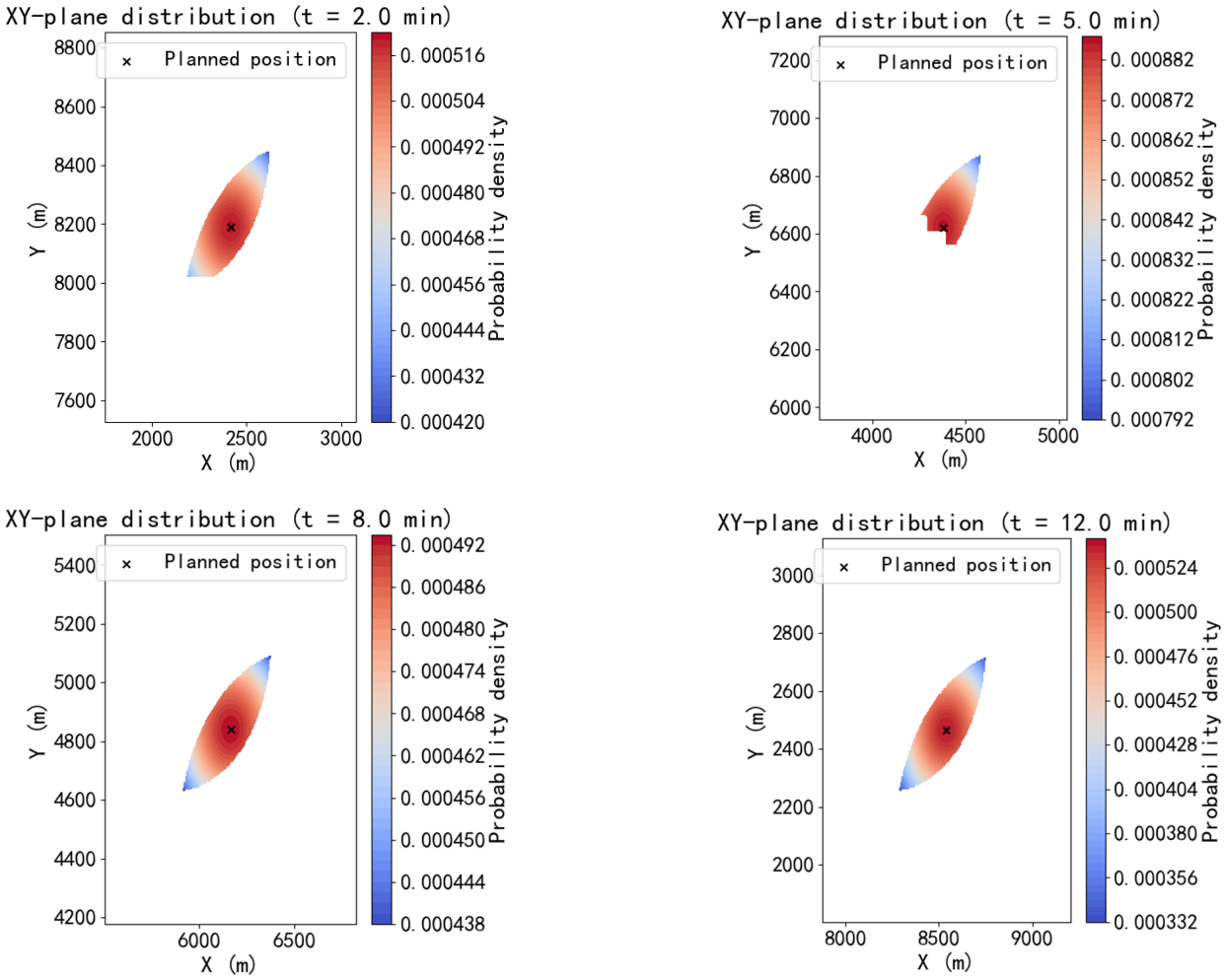


Figure 5. Probability distribution of drone positions in the xy plane.

Given that the probability values at individual coordinate points are small, we visualize the horizontal-plane distribution using a 50 m × 50 m grid for clarity. The numbers shown in the figure indicate the probability that the UAV visits each grid cell at the current time. The following plots present the UAV's positional probability distribution on the XY plane at different time instants. In particular, Figure 6 illustrates the visitation probability of different grid cells at the current moment, where the color scale from blue to red denotes increasing visitation probability.

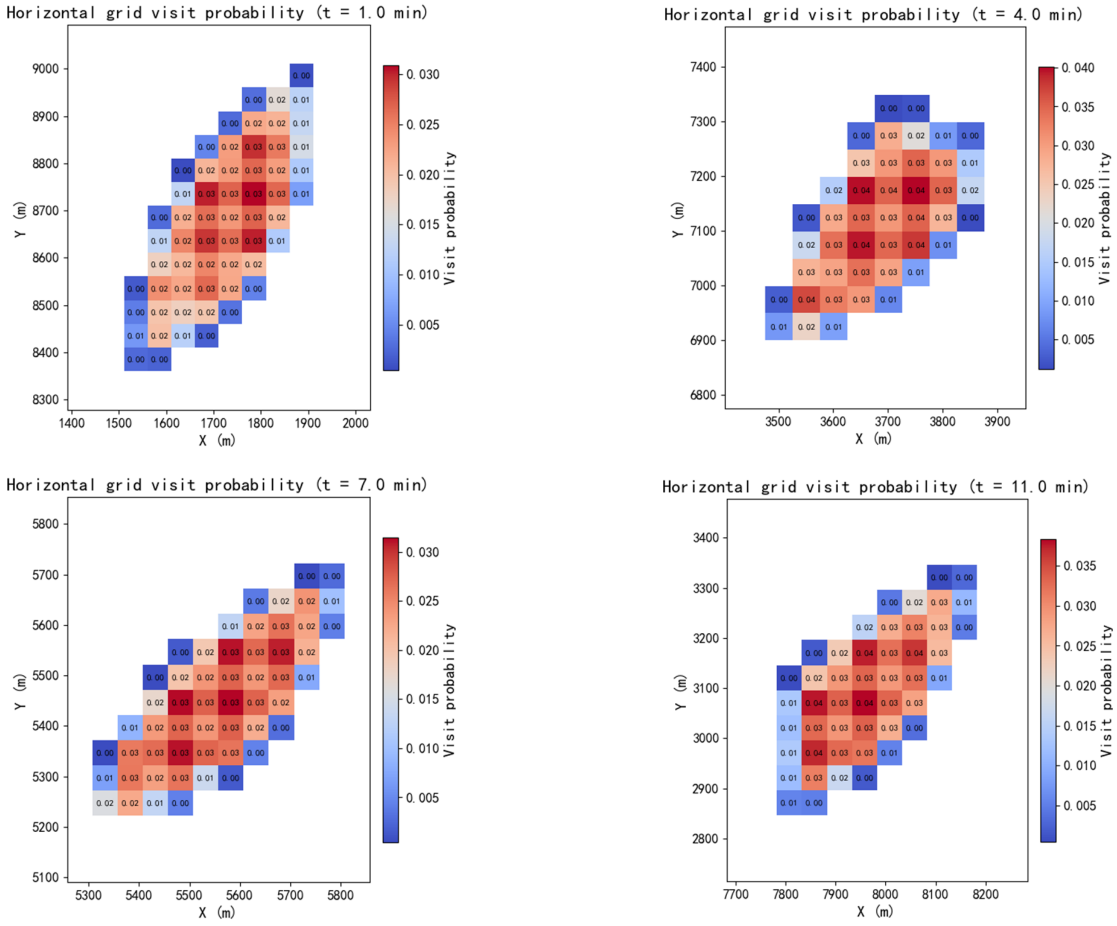


Figure 6. Rasterized probability distribution of the drone's position in the xy plane.

For the truncated normal distribution modeling of UAV altitude, the safety margin is set as $\Delta h_1 = 3$ m in the simulation, consistent with the previously defined vertical clearance. This means the lower bound of the UAV's flight altitude is $\mu_z(t) - 3$. Additionally, to limit excessive altitude that could lead to unnecessary energy consumption, the upper bound is set as $\mu_z(t) + 10$, with $\Delta h_2 = 10$ m. The Figure 7 below presents the altitude probability distribution of the UAV at various time instances. Since the shape of the truncated normal distribution remains consistent across different time steps, only the distribution at $t = 6$ min is shown here as a representative example.

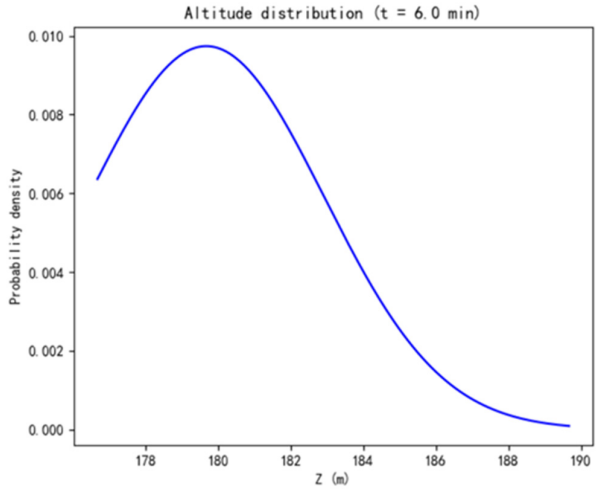


Figure 7. Probability distribution map of drone altitude.

Some of the parameters used in this experiment are shown in the following Table 1.

Table 1. Parameters Table.

Symbol/Name	Value	Unit
Horizontal cruise speed v_h	14	m/s
Max horizontal speed v_{max}	17	m/s
Horizontal acceleration a_h	4	m/s^2
Terrain clearance Δ_h	4	M
XY horizontal grid	200×200	Cells

4. Discussion

At this stage, the probabilistic position distribution of the UAV at any given moment during its mission has been established, both on the horizontal (XY) plane and along the vertical (Z) axis, thereby enabling the prediction of the UAV's probabilistic four-dimensional trajectory. To visualize the possible flight states, the Monte Carlo sampling method is employed, and the appropriate sample size n is determined through an RMSE-based convergence experiment. Specifically, n sample points are randomly extracted from the joint probability distribution at each time instant to generate the three-dimensional probabilistic trajectory distribution of the UAV. The probability of each sample point is computed according to Equation (22); regions where the samples are denser correspond to a higher likelihood of UAV presence.

To evaluate the convergence behavior of the Monte Carlo sampling process, an RMSE-based experiment was conducted by comparing the estimated empirical distribution $\hat{p}_n$ obtained from n sampled trajectories with the analytical reference distribution p^* on the same spatial grid. As shown in Figure 8, the root-mean-square error (RMSE) between $\hat{p}_n$ and p^* decreases rapidly with increasing n and then stabilizes beyond approximately $n = 400$. This result indicates that further increasing the sample count yields only marginal improvement in estimation accuracy while considerably raising computational cost. Therefore, $n = 400$ is adopted as a balanced choice between visualization smoothness and probabilistic accuracy.

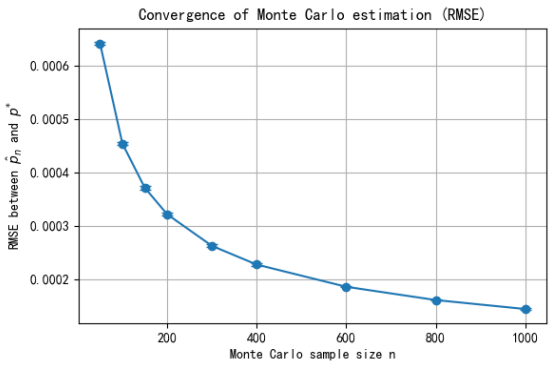


Figure 8. RMSE comparison experiment chart.

Finally, based on the obtained four-dimensional trajectory prediction results, multiple continuous 4D trajectories are generated as shown in Figure 9. By sampling the predicted trajectory at fixed time intervals from the UAV's position distribution, the sampled positions follow the Brownian bridge probability distribution. Regions that the UAV is more likely to pass through have higher visitation probabilities, and therefore a higher likelihood of being sampled. Subsequently, these discrete sampling points are interpolated and smoothed using stereo spline interpolation, and the physical performance limitations of the SF Ark 80 drone used in the example verification, such as the maximum flight speed, vertical and

horizontal acceleration, are taken into account to generate a four-dimensional trajectory sequence containing continuous time and spatial positions. The final visualization of the continuous 4D trajectories is shown in Figure 10 below. The image shows 20 different continuous four-dimensional trajectories, where lines of different colors represent different drone trajectories.

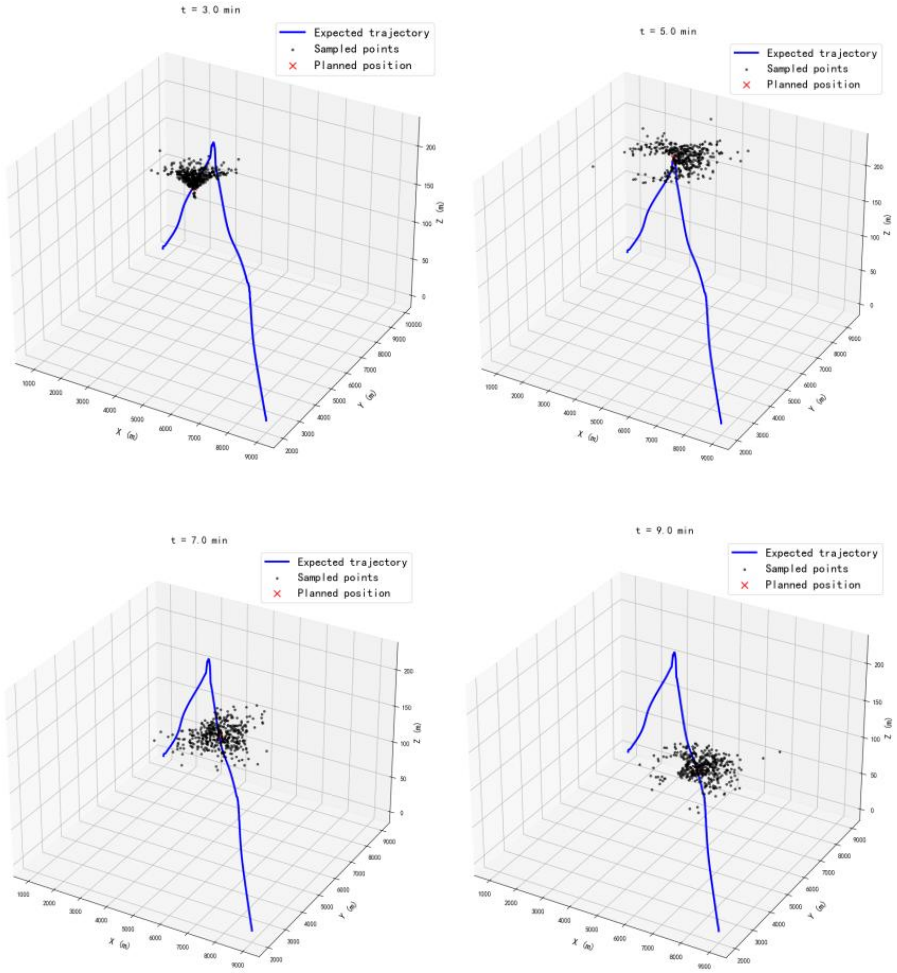


Figure 9. Schematic diagram of drone visit probability.

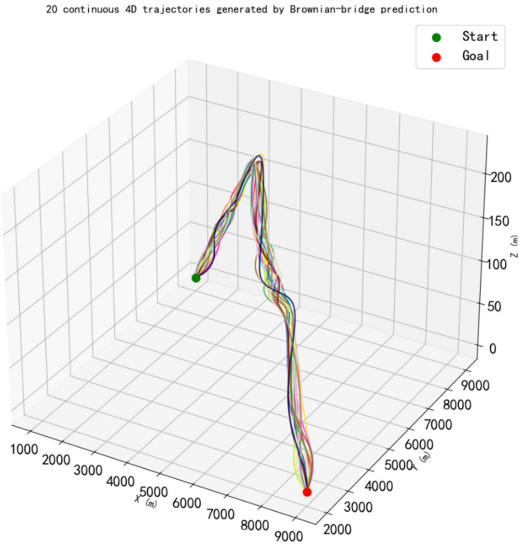


Figure 10. Schematic diagram of continuous four-dimensional trajectory prediction of the UAV.

From the final visualization of the continuous 4D trajectories, it can be observed that the UAV generally follows the originally planned trajectory. However, due to disturbances or uncertainties, the actual trajectory exhibits certain deviations at specific moments. Such deviations reflect the stochasticity and uncertainty of UAV operations in complex environments and also validate the effectiveness of the proposed Brownian bridge modeling approach in capturing the variation trends of UAV trajectories.

From a computational perspective, the main cost of the proposed framework arises from two key stages: three-dimensional path planning and probabilistic trajectory prediction. In the first stage, the improved A*-based planner searches the discretized 3D grid space and evaluates a composite heuristic function to efficiently identify an obstacle-free reference path. The computational load in this phase is primarily determined by the grid resolution and the geometric complexity of the terrain. Higher spatial resolution and more irregular topography increase the number of search nodes, but the jump-point and heuristic optimization mechanisms effectively reduce redundant expansions, maintaining a near-linear relationship between runtime and the number of grid cells. This process defines the initial trajectory topology and provides the boundary conditions for the subsequent probabilistic modeling.

In the second stage, the Brownian bridge-based trajectory prediction computes spatiotemporal probability distributions constrained by the reachable domain and terrain surface, generating continuous four-dimensional trajectories that capture the stochastic characteristics and dynamic uncertainty of UAV motion over time. The computational demand of this stage grows proportionally with the number of temporal discretization steps and the resolution of the probability field, both of which can be flexibly adjusted to balance computational cost and prediction accuracy.

Both stages exhibit near-linear scalability with respect to grid density and time resolution, ensuring that the framework remains tractable even for extended mission durations or complex flight environments. Moreover, since each UAV's trajectory can be predicted independently within its own spatiotemporal reachable domain, the framework naturally supports parallel computation and distributed processing. This enables efficient deployment in large-scale or multi-UAV operations without exponential growth in computational cost.

Overall, the proposed approach achieves a favorable balance between model fidelity, computational efficiency, and environmental adaptability, making it suitable for real-time or pre-tactical trajectory prediction and low-altitude UAV mission planning in diverse and complex terrain environments.

5. Conclusions

This paper proposes a probabilistic four-dimensional (4D) trajectory prediction model for unmanned aerial vehicles (UAVs) based on Brownian bridge motion, aiming to improve the accuracy and robustness of trajectory prediction during mission execution. In this model, the UAV's flight trajectory from the mission start point to the endpoint is treated as a Brownian bridge stochastic process with endpoint constraints. The UAV's path planning results are further incorporated as the expected path of the Brownian bridge, providing effective constraints for the prediction model.

At the same time, considering the UAV's spatiotemporal reachability during actual operations, a truncated probability distribution is employed to model and reflect the motion constraints imposed by performance and environmental limitations. Based on this framework, the model predicts UAV positional probabilities on both the horizontal plane and the vertical dimension, thereby achieving complete 4D probabilistic trajectory prediction. The resulting prediction outputs provide a continuous probabilistic representation of the UAV's

three-dimensional position at any moment during the mission, which is highly valuable for subsequent conflict probability estimation and tactical conflict detection tasks. Furthermore, by applying Monte Carlo sampling to the probabilistic trajectory distributions, a set of continuous and visually interpretable flight paths can be generated, effectively illustrating the stochastic characteristics and spatial dispersion of UAV trajectories throughout the mission. The Figure 11 below shows the continuous 4D trajectory of the drone in the geographical environment.

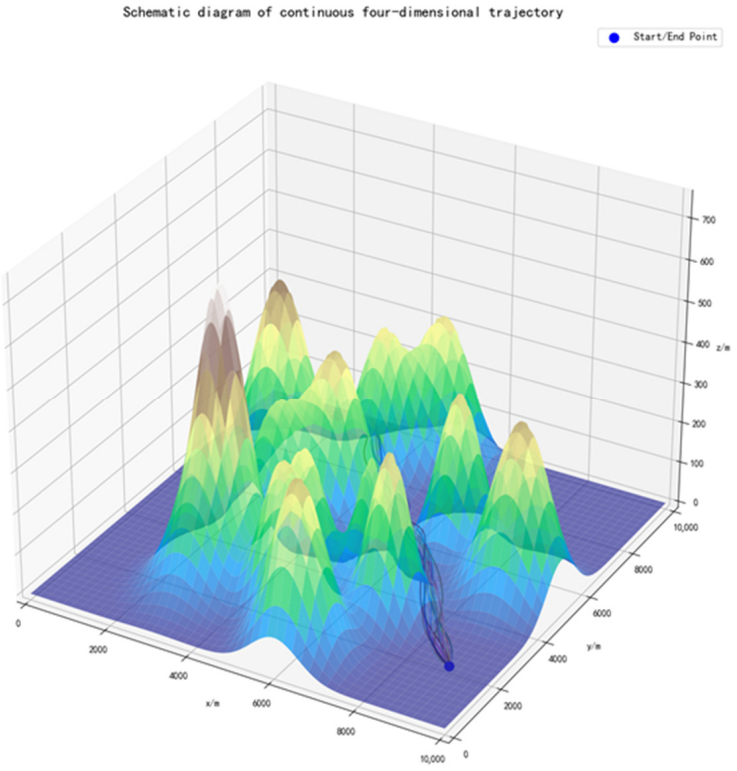


Figure 11. Schematic diagram of a continuous four-dimensional track on a topographic map.

Moreover, the proposed method is applicable to the pre-tactical phase of UAV missions, enabling probabilistic trajectory prediction in advance during mission planning. Such predictions not only support the identification and avoidance of potential conflicts but can also be applied to mission planning and optimization, the early detection and management of flight risks, and the development of emergency response plans. Consequently, the results of this study significantly enhance UAV flight safety, reliability, and operational efficiency and hold important theoretical and practical value for promoting safe and efficient UAV operations in complex low-altitude environments.

Author Contributions: Conceptualization, P.Z. and M.H.; methodology, P.Z. and Z.D.; software, P.Z.; validation, Z.D. and J.Y.; formal analysis, P.Z. and J.Y.; investigation, P.Z.; resources, P.Z. and M.H.; data curation, M.H.; writing—original draft preparation, P.Z. and Z.D.; writing—review and editing, P.Z. and M.H.; visualization, P.Z. and Z.D.; supervision, M.H. and J.Y.; project administration, M.H. and J.Y.; funding acquisition, M.H. All authors have read and agreed to the published version of the manuscript.

Funding: This research was funded by the National Natural Science Foundation of China (No. 52542206).

Institutional Review Board Statement: Not applicable.

Informed Consent Statement: Not applicable.

Data Availability Statement: The dataset is available from the authors upon request.

Conflicts of Interest: The authors declare no conflicts of interest.

References

1. Gao, Y.; Wang, X.; Zheng, D. Research on aircraft flight conflict risk prediction method in airport terminal area. *Chin. J. Saf. Sci.* **2017**, 157–162.
2. Yao, W. *UAVs Real-Time Mission Planning Based on Multi-Stage Track Prediction*; Harbin Institute of Technology: Harbin, China, 2015.
3. Xu, Z.; Zeng, W.; Yang, Z. Survey of civil aircraft trajectory prediction. *Comput. Eng. Appl.* **2021**, *57*, 65–74.
4. Kalantar, B.; Bin Mansor, S.; Halin, A.A.; Shafri, H.Z.M.; Zand, M. Multiple moving object detection from UAV videos using trajectories of matched regional adjacency graphs. *IEEE Trans. Geosci. Remote Sens.* **2017**, *55*, 5198–5213. [CrossRef]
5. Guerrero, J.S.G.; González, A.F.C.; Vega, J.I.H.; Tovar, L.A.N. Instrumentation of an array of ultrasonic sensors and data processing for unmanned aerial vehicle (UAV) for teaching the application of the Kalman filter. *Procedia Comput. Sci.* **2015**, *75*, 375–380. [CrossRef]
6. Ho, T.D.; Grotli, E.I.; Johansen, T.A. Pso and kalman filterbased node motion prediction for data collection from ocean wireless sensors network with UAV. In Proceedings of the 2021 IEEE International Conference on Consumer Electronics (ICCE), Las Vegas, NV, USA, 10–12 January 2021.
7. Wang, Y.; Chen, K. Hypersonic target interception based on shortrange damage estimation. *J. Phys. Conf. Ser.* **2023**, *2478*, 102007. [CrossRef]
8. Kant, R.; Saini, P.; Kumari, J. Long Short-Term Memory AutoEncoder-Based Position Prediction Model for Fixed-Wing UAV During Communication Failure. *IEEE Trans. Artif. Intell.* **2022**, *4*, 173–181. [CrossRef]
9. Hong, D.; Lee, S.; Cho, Y.H.; Baek, D.; Kim, J.; Chang, N. Leastenergy path planning with building accurate power consumption model of rotary unmanned aerial vehicle. *IEEE Trans. Veh. Technol.* **2020**, *69*, 14803–14817. [CrossRef]
10. Cui, S.; Chen, Y.; Li, X. A Robust and Efficient UAV Path Planning Approach for Tracking Agile Targets in Complex Environments. *Machines* **2022**, *10*, 931. [CrossRef]
11. Huang, Y.; Du, J.; Yang, Z.; Zhou, Z.; Zhang, L.; Chen, H. A survey on trajectory-prediction methods for autonomous driving. *IEEE Trans. Intell. Veh.* **2022**, *7*, 652–674. [CrossRef]
12. Zhao, Y.; Yang, M. Unmanned aerial vehicle trajectory prediction based on operating state recognition. *Sci. Technol. Eng.* **2019**, *19*, 304–309.
13. Zhang, H.; Yan, Y.; Li, S.; Hu, Y.; Liu, H. UAV behavior-intention estimation method based on 4-D flight-trajectory prediction. *Sustainability* **2021**, *13*, 12528. [CrossRef]
14. Hwang, I.; Hwang, J.; Tomlin, C. Flight-mode-based aircraft conflict detection using a residual-mean interacting multiple model algorithm. In Proceedings of the USA: AIAA Guidance, Navigation, and Control Conference and Exhibit, Austin, TX, USA, 11–14 August 2003; AIAA: Reston, VA, USA, 2003; p. 5340.
15. Yepes, J.L.; Hwang, I.; Rotea, M. New algorithms for aircraft intent inference and trajectory prediction. *J. Guid. Control. Dyn.* **2007**, *30*, 370–382. [CrossRef]
16. Liu, W.; Hwang, I. Probabilistic trajectory prediction and conflict detection for air traffic control. *J. Guid. Control. Dyn.* **2011**, *34*, 1779–1789. [CrossRef]
17. Zhang, J.; Wu, X.; Wang, F. Aircraft trajectory prediction based on modified interacting multiple model algorithm. *J. Donghua Univ. Engl. Ed.* **2015**, *32*, 180–184.
18. Seah, C.E.; Hwang, I. Hybrid estimation algorithm using state-dependent mode transition matrix for aircraft tracking. In Proceedings of the USA: AIAA Guidance, Navigation and Control Conference, Keystone, CO, USA, 21–24 August 2006. [CrossRef]
19. Zhang, J.; Sui, D.; Tang, X. Aircraft trajectory prediction based on SDTHE algorithm. *Syst. Eng. Theory Pract.* **2014**, *34*, 2955–2964.
20. Zhong, G.; Zhang, H.; Zhou, J.; Zhou, J.; Liu, H. Short-term 4D trajectory prediction for UAV based on spatio-temporal trajectory clustering. *IEEE Access* **2022**, *10*, 93362–93380. [CrossRef]
21. Ma, L.; Tian, S. A hybrid cnn-LSTM model for aircraft 4d trajectory prediction. *IEEE Access* **2020**, *8*, 134668–134680. [CrossRef]
22. Munaye, Y.Y.; Lin, H.-P.; Adege, A.B.; Tarekegn, G.B. UAV positioning for throughput maximization using deep learning approaches. *Sensors* **2019**, *19*, 2775. [CrossRef]
23. Zhang, Y.; Jia, Z.; Dong, C.; Liu, Y.; Zhang, L.; Wu, Q. Recurrent LSTM-based UAV Trajectory Prediction with ads-b Information. In Proceedings of the GLOBECOM 2022—2022 IEEE Global Communications Conference, Rio de Janeiro, Brazil, 4–8 December 2022; IEEE: New Work, NY, USA, 2022; pp. 1–6. [CrossRef]
24. Zhang, B.; Yang, P.; Liang, Y.; Bai, Z.; Zhu, W. Real-time track prediction of air combat UAV based on LSTM. *Tactical Missile Technol.* **2024**, *3*, 72–83.
25. Barratt, S.T.; Kochenderfer, M.J.; Boyd, S.P. Learning probabilistic trajectory models of aircraft in terminal airspace from position data. *IEEE Trans. Intell. Transp. Syst.* **2018**, *20*, 3536–3545. [CrossRef]

26. Ayhan, S.; Samet, H. Aircraft trajectory prediction made easy with predictive analytics. In Proceedings of the 22nd ACM SIGKDD International Conference on Knowledge Discovery and Data Mining, San Francisco, CA, USA, 13–17 August 2016. [CrossRef]
27. Siqi, H. *Research on Aircraft Conflict Detection and Resolution Under Four-Dimensional Trajectory-Based Operation*; Harbin Institute of Technology: Harbin, China, 2020.
28. Hu, C.; Niu, R.; Lin, Y.; Yang, B.; Chen, H.; Zhao, B.; Zhang, X. Probabilistic trajectory prediction of vulnerable road user using multimodal inputs. *IEEE Trans. Intell. Transp. Syst.* **2025**, *26*, 2679–2689. [CrossRef]
29. Pepper, N.; De Ath, G.; Carvell, B.; Hodgkin, A.; Dodwell, T.; Thomas, M.; Everson, R. A sector-specific probabilistic approach for 4D aircraft trajectory generation. *Transp. Res. Part C Emerg. Technol.* **2025**, *179*, 105291. [CrossRef]
30. Xiang, J.; Chen, J. Data-driven probabilistic trajectory learning with high temporal resolution in terminal airspace. *J. Aerosp. Inf. Syst.* **2025**, *22*, 682–692. [CrossRef]
31. Westny, T.; Olofsson, B.; Frisk, E. Diffusion-based environment-aware trajectory prediction. *arXiv* **2024**, arXiv:2403.11643.
32. Postnikov, A.; Gamayunov, A.; Ferrer, G. Transformer based trajectory prediction. *arXiv* **2021**, arXiv:2112.04350. [CrossRef]
33. Federal Aviation Administration (FAA). Unmanned Aircraft System Traffic Management (UTM). Available online: https://www.faa.gov/uas/advanced_operations/traffic_management (accessed on 14 October 2025).
34. Yan, S.; Shi, X.; Zhang, Z. Three-dimensional path planning of urban logistics UAVs. *Sci. Technol. Eng.* **2024**, *24*, 12781–12788.
35. Winter, S.; Yin, Z.C. The elements of probabilistic time geography. *Geoinformatica* **2010**, *15*, 417–434. [CrossRef]

Disclaimer/Publisher's Note: The statements, opinions and data contained in all publications are solely those of the individual author(s) and contributor(s) and not of MDPI and/or the editor(s). MDPI and/or the editor(s) disclaim responsibility for any injury to people or property resulting from any ideas, methods, instructions or products referred to in the content.